Dehydrogenation free energy of Co^{2+}(aq) from density functional theory-based molecular dynamics

Hodel, Florian H ; Luber, Sandra

Abstract: Electron and proton transfers are important steps occurring in chemical reactions. The often used approach of calculating the energy differences of those steps using methods based on geometry optimizations neglects the influence of dynamic effects. To further investigate this issue and inspired by research in water oxidation, we calculate in the present study the dehydrogenation free energy of aqueous Co2+, which is the free energy change associated with the first step of the water oxidation reaction mechanism of recently investigated model Co(II)-aqua catalysts. We employ a method based on a thermodynamic integration scheme with strong ties to Marcus theory to obtain free energy differences, solvent reorganization free energies, and dynamic structural information on the systems from density functional theory-based molecular dynamics. While this method is computationally orders of magnitude more expensive than a static approach, it potentially allows for predicting the validity of the approximation of neglecting dynamic effects.

DOI: https://doi.org/10.1021/acs.jctc.6b01077

Originally published at:
Hodel, Florian H; Luber, Sandra (2017). Dehydrogenation free energy of Co^{2+}(aq) from density functional theory-based molecular dynamics. Journal of Chemical Theory and Computation, 13(3):974-981.
DOI: https://doi.org/10.1021/acs.jctc.6b01077

Dehydrogenation Free Energy of Co^{2+}(aq) from Density Functional Theory-based Molecular Dynamics

*Florian H. Hodel, Sandra Luber**

Department of Chemistry, University of Zurich, Winterthurerstrasse 190, CH-8057 Zurich, Switzerland

ABSTRACT Electron and proton transfers are important steps occurring in chemical reactions. The often used approach of calculating the energy differences of those steps using methods based on geometry optimizations neglects the influence of dynamic effects. To further investigate this issue and inspired by research in water oxidation, we calculate in the present study the dehydrogenation free energy of aqueous Co^{2+}, which is the free energy change associated with the first step of the water oxidation reaction mechanism of recently investigated model Co(II)-aqua catalysts. We employ a method based on a thermodynamic integration scheme with strong ties to Marcus theory to obtain free energy differences, solvent reorganization free energies, and dynamic structural information on the systems from density functional theory-based molecular dynamics. While this method is computationally orders of magnitude more expensive than a static approach, it potentially allows to predict the validity of the approximation of neglecting dynamic effects.

Introduction

Hydrogen production by photocatalytic water splitting is a promising approach to satisfy the ever increasing demand for sustainable fuels.[1,2] With the oxidation half reaction being the limiting factor of this process,[3] the development of efficient and cheap water oxidation catalysts (WOCs) is paramount. Kanan and Nocera's report of a cobalt oxide ("artificial leaf") WOC[4] has triggered many studies on Co(III) and especially Co(III) containing cubanes as catalysts for water oxidation.[5-12] However, there has been a debate on whether water oxidation activity by those Co(III)-cubanes might be due to free Co(II) ions present as impurities or from the decomposition of the cubane catalysts.[13,14]

Contributing to the elucidation of this issue, Patzke and coworkers reported that $CoCl_2$ and $CoBr_2$ at low pH (to prevent the formation of oxide clusters) do in fact display water oxidation activity.[15] Inspired by these observations, Schilling *et al*. computationally investigated two potential water oxidation mechanisms of an octahedral model complex $[Co^{II}(H_2O)_6]^{2+}$.[16] Apart from a water-nucleophilic-attack and the release of O_2 at the end of the cycles, all catalytic states were assumed to be connected by proton coupled electron transfer (PCET) steps. Therefore, free energy differences between those states were calculated employing an approach by Nørskov *et al*.,[17-20] in which only the free energy of the electron-proton pair, not the individual chemical potential needs to be calculated. This method entails several approximations: firstly, it is assumed that the PCET steps occur with no barrier, secondly, dynamic effects are considered to be of negligible influence, and finally, by construction, proton and electron transfer always occur simultaneously.

In the present study, we investigate these points more closely and, to this end, report calculations of the dehydrogenation free energy of the above mentioned aqueous Co(II) ion, i.e. the PCET reaction

$$[Co^{II}(H_2O)_6]^{2+}(aq) \rightarrow [Co^{III}(H_2O)_5OH]^{2+}(aq) + ½\ H_2(g)\ , \qquad (1)$$

using Kohn-Sham density functional theory (DFT)[21,22] in a molecular dynamics (MD) approach pioneered by Sprik and coworkers,[23-31] which is based on a free energy perturbation scheme.[32,33] This first step of the catalytic cycle of water oxidation by aqueous Co(II) ions also serves us as a model system for more complex WOCs such as Co(II)-based cubanes,[34,35] the water oxidation mechanisms of which we had investigated previously.[36-38]

DFT-MD, which applies the same level of theory to all atoms of the system, provides potentially more accurate results for such studies than the popular implicit solvent approaches[39,40] due to its ability to capture also intricate effects such as solvent reorganization.[30] The computational cost is however substantial. In this work, the two half reactions (oxidation and deprotonation) were treated separately and the free energies were calculated by reversible insertion of protons and electrons. More precisely, we obtained free energy differences by thermodynamic integration (TI) of vertical energy gaps between diabatic surfaces including a number of thermochemical corrections, which is a free energy perturbation scheme that has strong connections to Marcus theory.[27,41-45]

Methods

A thorough review of the theory behind the method employed, as well as a detailed description of every step of our calculations can be found in the SI. We therefore give here only a brief overview and report the set-up parameters used in the simulations.

The systems we calculate in our TI approach are described by Hamiltonians that are given by linear combinations of the Hamiltonians of the reactant and product states (0 and 1) of the reactions under investigation. Therefore, the potential energy surfaces on which we sample are given by[46,47]

$$E(\eta, \mathbf{x}) = E_0(\mathbf{x}) + \eta\big(E_1(\mathbf{x}) - E_0(\mathbf{x})\big), \qquad \eta \in [0,1] \tag{2}$$

with a coupling parameter η and a vector $\mathbf{x}$ describing the systems' configuration.

We first removed an electron from the aqueous cobalt ion and approximated the oxidation integral $\Delta_{\mathrm{ox}}A$ assuming linear solvent response as

$$\Delta_{\mathrm{ox}}A = \int_0^1 \langle \Delta_{\mathrm{ox}}E \rangle_\eta \, d\eta \approx \frac{\langle \Delta E \rangle_0 + \langle \Delta E \rangle_1}{2} \tag{3}$$

with $\langle \Delta E \rangle_\eta$ denoting the ensemble average of the vertical energy gap $\Delta E(\mathbf{x}) = E_1(\mathbf{x}) - E_0(\mathbf{x})$ for the coupling parameter η.

We investigated the proton transfer from $[Co^{III}(H_2O)_6]^{3+}$ by alchemically transforming one of the protons ($\eta = 0$) into a dummy atom ($\eta = 1$) (i.e. turning off all interactions with other atoms). Since for such a process the solvent response is likely to be non-linear, intermediate states ($\eta = 0.25, 0.5, 0.75$) were included, and the deprotonation integral can be approximated as

$$\begin{aligned}\Delta_{\mathrm{dp}}A &= \int_0^1 d\eta\, \langle \Delta_{\mathrm{dp}}E \rangle_{r\eta} \\ &\approx \frac{1}{12}\left(\langle \Delta_{\mathrm{dp}}E \rangle_{r,0} + \langle \Delta_{\mathrm{dp}}E \rangle_{r,1}\right) + \frac{1}{6}\langle \Delta_{\mathrm{dp}}E \rangle_{r,0.5} \\ &+ \frac{1}{3}\left(\langle \Delta_{\mathrm{dp}}E \rangle_{r,0.25} + \langle \Delta_{\mathrm{dp}}E \rangle_{r,0.75}\right).\end{aligned} \tag{4}$$

To avoid high-energy conformations upon proton insertion, we restrained the position of the dummy atom to the one of the original proton with a restraining potential V_r. This is denoted in equation 4 with a subscript r.

Due to the uncertainty in the reference of the electrostatic potential for charged periodic systems $\Delta_{\mathrm{ox}}A$ and $\Delta_{\mathrm{dp}}A$ cannot be compared to experimental values. However, the deprotonation free energy can be calculated as[28]

$$\Delta_{\mathrm{dh}}G = \Delta_{\mathrm{ox}}A + \Delta_{\mathrm{dp}}A - \Delta_{\mathrm{f}}G_{\mathrm{H}^+(g)} - \Delta A_{\mathrm{corr}} \tag{5}$$

where $\Delta_{\mathrm{f}}G_{\mathrm{H}^+(g)}$ is the free energy of formation of a proton in gas phase, and ΔA_{corr} is a correction term, the individual components of which are reported in Table 1 in section Results (see also SI for a more thorough derivation and description of the methods and approximations made).

Computational Set-Up

The DFT-MD calculations were carried out with the QUICKSTEP program[48] as implemented in the CP2K package,[49] which uses a mixed Gaussian and plane wave scheme with the wave functions expanded in terms of a Gaussian basis set and the charge density represented with an auxiliary plane wave basis.

All systems consisted of $Co^{II}(H_2O)_6$ or $Co^{III}(H_2O)_5OH$ and 82 water molecules in a periodic cubic box. $Co^{II}(H_2O)_6$ was equilibrated by first running 1 ns of classical MD with the coordinates of the solute fixed, followed by 4 ps of DFT-MD, both in the NpT ensemble. Furthermore, we

generated several DFT-MD trajectories in the NVT ensemble with slightly changed volumes and monitored the pressure. With the in this way obtained box size of 13.63^3 Å^3, we equilibrated all systems for another 12-15 ps of DFT-MD in the NVT ensemble. We used a timestep of 0.5 fs and the temperature was held around 300 K by a canonical sampling through velocity rescaling (CSVR) thermostat[50] for each degree of freedom ("massive thermostatting") with a time constant of 10 fs. For the simulations in the isothermal-isobaric ensemble, the external pressure was set to 1 bar and the time constant of the barostat to 100 fs. The classical MD simulations were carried out using the CHARMM force field,[51] TIP3P water model,[52] and a time constant of 1000 fs for both thermostat and barostat. The charges of the systems were neutralized by a negative background charge, which, while an entirely artificial feature, introduces less bias than explicit counter ions in "infinite dilution" systems the size of ours.[53]

Subsequently, in the production runs, we sampled for up to 30 ps in the NVT ensemble. The exact lengths of each trajectory are displayed in Figures 1 and 2 in section Results. The thermostat was coupled to the whole system ("global thermostatting") and its time constant increased to 50 fs. The potential energy surfaces $E(\eta, \mathbf{x})$ (see equation (2)) were sampled employing the "multiple force-eval" environment of CP2K, and the forces used to generate configurations were obtained with contributions from two Hamiltonians corresponding to $\eta = 0$ and $\eta = 1$, respectively.

The energies (and forces) were calculated using the BP86 exchange-correlation (XC) functional, which has been shown to deliver reliable structures of transition metal complexes in static, as well as dynamic (DFT-MD) calculations.[54-60] We employed DZVP-MOLOPT-GTH basis sets,[61] a 400 Ry cutoff for the auxiliary plane wave expansion of the charge density, and Goedecker-Teter-Hutter (GTH) norm-conserving pseudopotentials to represent the core

electrons.[62,63] Kohn-Sham and overlap matrix elements smaller than $\varepsilon_{default}=10^{-12}$ were neglected, and the convergence criterion for the electronic gradient (largest element of the gradient) was set to $\varepsilon_{SCF}=10^{-6}$. Moreover, we included the D3 dispersion correction by Grimme *et al.*,[64] which has been shown to be necessary for a correct description of transition metal complexes,[65] as well as to (partially) remedy the well-known issue of over-structuring of water by generalized-gradient approximation (GGA) exchange-correlation (XC) functionals.[66-69] With the set-up described above, we observed for the production runs a drift in total energy between 10^{-6} and 10^{-5} eV/ps/atom.

The restraining potential V_r which was added to the potential energy function $E(\eta, \mathbf{x})$ was chosen as

$$V_r = \frac{k_r}{2}(r - r_{eq})^2 + \frac{k_\theta}{2}(\theta - \theta_{eq})^2 + \frac{k_\xi}{2}(\xi - \xi_{eq})^2 \ , \qquad (6)$$

where k_r, k_θ and k_ξ are force constants, r is the distance O-H_{dum}, θ is the angle H-O-H_{dum}, ξ is the angle Co-O-H_{dum} and $r_{eq} = 1.009$ Å, $\theta_{eq} = 108.32°$ and $\xi_{eq} = 115.29°$ are their equilibrium values. We obtained these equilibrium values by calculating averages over an DFT-MD trajectory of the $[Co^{III}(H_2O)_6]^{3+}$-system. We chose the force constants so that the maximal force exerted by the harmonic potential would not exceed 0.02 a.u. While a balance between counteracting thermal fluctuations and overly biasing the free energies has to be found, their precise values are not crucially important and we therefore set them all to the same value of 0.1 a.u.[28,70,71]

Using geometry optimizations with different total spin multiplicities, we determined the lowest energy spin states of our systems. To this end, we employed the same set-up as the DFT-MD calculations described above and determined Co(II) to prefer a high spin and Co(III) a low spin

configuration, which agrees not only with other DFT studies,[72] but also with experimental findings on these aqua complexes.[73,74] This is the reason why we did neither directly calculate the dehydrogenation integral for an alchemical process involving the simultaneous removal of a proton and an electron, nor first the deprotonation followed by oxidation (according to Hess' law, all three approaches should deliver the same dehydrogenation free energy). Since, as mentioned above, linear solvent response cannot be assumed for dehydrogenation and deprotonation, sampling only the corresponding endstates does not suffice. In general, they not only need more intermediate states than calculations of oxidation reactions, the expectation value of the vertical energy gap also converges more slowly, which means that the trajectories need to be longer.[28] By first oxidizing Co(II) to Co(III), only two MD simulation require spin-polarized calculations, and all others (corresponding to the deprotonation reaction) can be carried out with a closed-shell approach at lower computational cost.

Results

As mentioned in the introduction, we split the dehydrogenation reaction (equation (1)) into an oxidation, followed by a deprotonation reaction. Aside from the calculations of the correction terms, the ensemble averages of the vertical energy gaps ΔE are the only things needed in our TI scheme to obtain the oxidation and deprotonation integrals ($\Delta_{\mathrm{ox}}A$ and $\Delta_{\mathrm{dp}}A$, respectively) and from them the dehydrogenation free energy $\Delta_{\mathrm{dh}}G$. In the following, we will discern between time averages $\overline{\Delta E}$ and ensemble averages $\langle \Delta E \rangle$, which are, assuming ergodicity for our systems, equal for long enough DFT-MD trajectories.

Vertical Energy Gaps

The accumulative time averages of the energy gaps in the reduced (Co^{II}) ($\eta = 0$) and the oxidized (Co^{III}) states ($\eta = 1$) are shown Figure 1. Taking their values at the end of the trajectories as ensemble averages, we obtain $\Delta_{ox}A = 0.80$ eV according to equation (3). To get an idea of the reliability of this value we will investigate below whether the deviations of our system from a linear solvent response are significant.

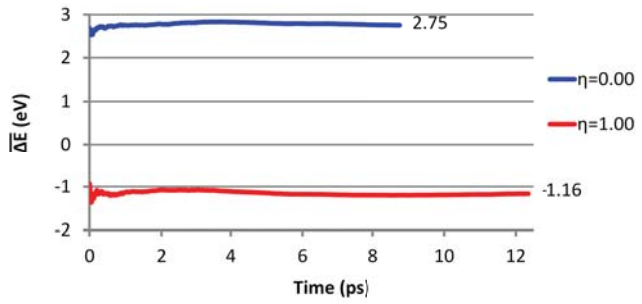

Figure 1: Accumulative time averages of the vertical energy gaps of the oxidation reaction. $\eta = 0$ corresponds to the reduced, $\eta = 1$ to the oxidized limit.

For the deprotonation reaction, we sampled not only in the protonated ($\eta = 0$) and deprotonated states ($\eta = 1$), but also in three unphysical intermediate ones (see Figure 2).

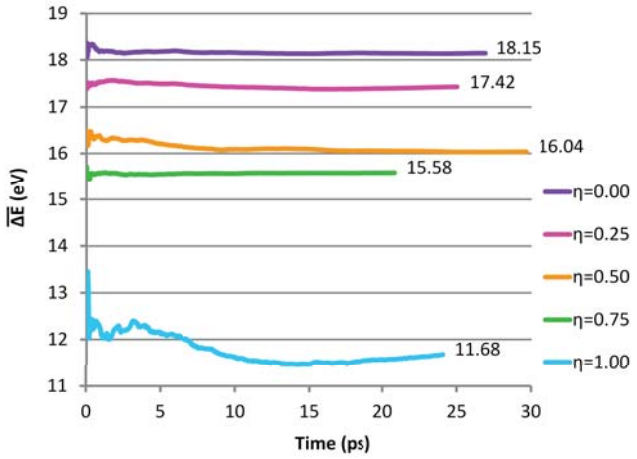

Figure 2: Accumulative time averages of the vertical energy gaps of the deprotonation reaction. $\eta = 0$ corresponds to the protonated, $\eta = 1$ to the deprotonated limit.

It is apparent that assuming the system to be in the linear regime would not have been appropriate. The ensemble averages of the vertical energy gaps are not equally spaced, but are separated into three groups. In the deprotonated limit, the vertical energy gap converges more slowly than in the other states and fluctuates more, which is due to the problems of calculating insertion energies in the condensed phase (see SI, section Calculation of Adiabatic Free Energy Differences). From the ensemble averages of the energy gaps presented in Figure 2, we obtain $\Delta_{\mathrm{dp}}\mathrm{A} = 16.16\ \mathrm{eV}$ using equation (4). Due to the uncertainty in the reference of the electrostatic potential, $\Delta_{\mathrm{dp}}\mathrm{A}$ and $\Delta_{\mathrm{ox}}\mathrm{A}$ can however not be compared to experimental acidity constants or redox potentials. Nevertheless, including appropriate corrections and the free energy of solvation of a proton, we can calculate $\Delta_{\mathrm{dh}}G$ for their sum (see equation (5)).

Table 1: Corrections included in the final dehydrogenation free energy.[a]

Correction term		[meV]
dissociation entropy	$-k_B T ln\left[c^{\circ} \Lambda_{H^+}^3\right]$	190.1
rotational partition function ratio	$-k_B T ln[f_{dum}^{rot}]$	-0.5
vibrational partition function ratio	$-k_B T ln\left[f_{dum}^{vib,ZPE}\right]$	-5.2
zero-point energy	ΔE_{ZPE}	248.5
configurational entropy	$k_B T ln[6]$	46.0
total	ΔA_{corr}	478.9

[a] For their derivation see SI, section Correction Terms.

The explicit values of all correction terms (see equation (5)) are listed in Table 1. The most important contributions come from the zero-point energy, the dissociation entropy and the configurational entropy. Overall, the dehydrogenation free energy amounts to $\Delta_{\mathrm{dh}} G = 0.67$ eV.

Since there is no experimental value to compare with, we used a different computational protocol to calculate the dehydrogenation free energy using an implicit solvent model and the same exchange-correlation functional but different basis sets in a non-periodic framework (see SI, section Thermodynamic Cycle for further details). Employing this approach, we obtained a dehydrogenation free energy of $\Delta_{\mathrm{dh}} G^{\circ} = 1.70$ eV. This value was calculated as the sum of the free energy associated with the proton transfer and the electron transfer, each of them calculated individually. Comparing the calculated reduction potential of $[Co^{II}(H_2O)_6]^{2+}$ of 0.70 V and the calculated acid dissociation constant (pK_a) of $[Co^{III}(H_2O)_6]^{3+}$ (16.9) approximately with the corresponding experimental values of 1.82 V[75] and 2.92,[76] respectively, reveals that the underlying assumptions and errors of this protocol also deserve an in-depth evaluation, which is however beyond the scope of the present work. Several improvement options have been suggested and we refer to recent reviews in Refs. [77,78].

Testing for Linear Solvent Response

A necessary condition for a linear solvent response is that the probability distributions of the energy gaps in the two endstates be of Gaussian type with the same width, i.e. the samplings of the vertical energy gaps in states $\eta = 0$ and $\eta = 1$ have the same variance. From this variance, the reorganization energy can be calculated and compared to the value obtained from the vertical energy gap averages with equation (S32) in the SI. For the oxidation reaction, the difference in the standard deviations of the two Gaussian distributions is 70 meV (see Figure 3) which leads to unequal reorganization free energies of $\lambda_{0(R)} = 1.07$ eV in the reduced and $\lambda_{1(O)} = 1.79$ eV in the oxidized state. They furthermore differ from the value obtained by taking the difference between half of the average vertical energy gaps of the reduced and the oxidized state (1.96 eV) (see equation (S32)).

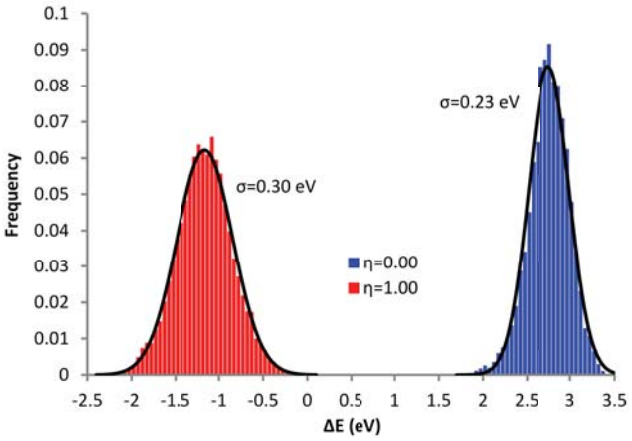

Figure 3: Distributions of the vertical energy gaps of the oxidation reaction with Gaussian distributions (black) fitted to the data. $\eta = 0$ corresponds to the reduced, $\eta = 1$ to the oxidized limit, σ denotes the standard deviation of the distributions.

The unequal distributions and reorganization energies are not necessarily a cause for concern, since firstly, variances (and reorganization energies) converge more slowly than expectation values and might not be fully converged within our DFT-MD durations,[28] and secondly, it has been shown that the differences between adiabatic free energy gaps obtained with the assumption of linear solvent response, and calculated by additionally sampling in intermediate states are small even for significantly differing vertical energy gap distributions.[79] More specifically, it has been reported (for an ion solvated with a classical simple point charge water model) that for a difference in standard deviations of 0.13 eV, which even went along with a change in the number of water molecules in the first solvation shell (see below), assuming linear solvent response changed the oxidation free energy by less than 5%.[78] It appears that equation (3) is robust and provides in many cases a good estimate of $\Delta_{\mathrm{ox}}\mathrm{A}$.[23,33,80]

Judging by the time evolutions of $\langle \Delta_{\mathrm{dp}} E \rangle_{r\eta}$ of the deprotonation reaction, it is unsurprising that their distributions in the protonated and deprotonated state displayed in Figure 4 are dissimilar. The standard deviations differ by 1.67 eV, and in the deprotonated limit, the distribution is no longer Gaussian indicating a significant departure from the linear regime. In this case, calculating the reorganization energy from the variance is not an appropriate approximation. However, with equations (S28) and (S29) in the SI, we obtain $\lambda_{0(prot)} = 4.48$ eV and $\lambda_{1(dp)} = 1.99$ eV.

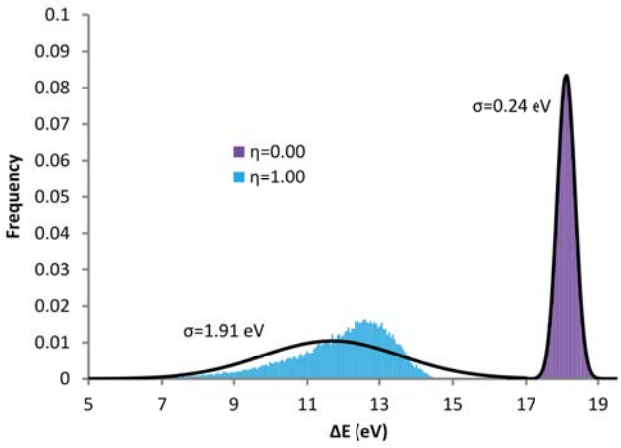

Figure 4: Distributions of the vertical energy gaps of the deprotonation reaction with Gaussian distributions (black) fitted to the data. $\eta = 0$ corresponds to the protonated, $\eta = 1$ to the deprotonated limit.

Correlations Between Vertical Energy Gaps and the Solvent Structure

The structure of the solvation shell during oxidation can be visualized by plotting the radial distribution function (RDF) between the cobalt ion and all oxygen atoms (Figure 5). The $Cu^{2+}(aq)|Cu^{+}(aq)$ redox reaction, for example, has been found to go along with a change in the Cu-(H_2O) coordination number, which led to strong deviations from the linear regime.[81]

Firstly, it should be noted that in the reduced state, as expected for a high-spin d^7 complex, Jahn-Teller distortions due to the spatially degenerate electronic ground state are weak because for symmetry reasons, the unevenly occupied t_{2g} orbitals are less involved in the σ-bonding than the e_g level.[82-84] For Co(III), low-spin d^6, there is no Jahn-Teller effect. Hence, uneven Co-O bond lengths at a given snapshot of a trajectory can be attributed primarily to thermal fluctuations and solute-solvent interactions.

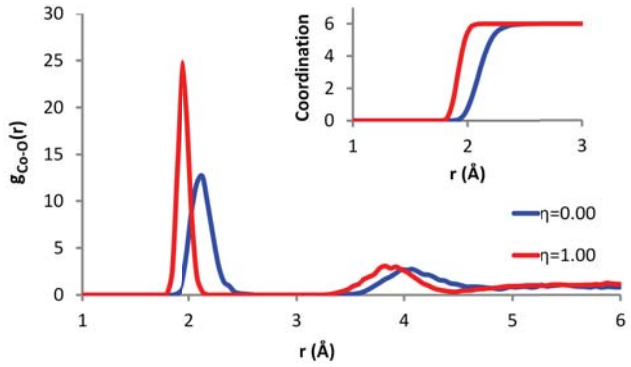

Figure 5: Large graph: RDFs between cobalt and oxygen of the reduced ($\eta = 0$) and the oxidized ($\eta = 1$) state. Inset: Integral of the RDFs.

In the oxidized state ($\eta = 1$), the Co-O bond lengths are slightly shorter than in $[Co^{II}(H_2O)_6]^{2+}$ ($\eta = 0$) and fluctuate less during the corresponding MD simulation, which manifests itself in a narrowed first peak of the RDF being shifted to left in Figure 5. Based on the fact that the metal-ligand interactions are mostly electrostatic, the shortened bond length in the more oxidized Co complex is unsurprising.[85] The coordination number (i.e. the integral of the radial distribution function $g(r)$ from 0 to the first minimum) is not changed by the removal of an electron. Overall, the Co-O RDF changes only insignificantly upon oxidation, which is in line with our assumption of a linear solvent response.

So far, we only looked at the positions of the oxygen atoms relative to Co. However, this does not provide us with information about the hydrogen bond (H-bond) network. To further investigate the solvent structure, we therefore also calculated the RDF between the 6 oxygen atoms directly bound to Co and the hydrogen atoms of the solvating water molecules (H_w, see upper part of Figure 6). As could be expected based on steric considerations alone, the number of H-bonds donated to the water ligands is small. After the oxidation it has decreased from an average of 0.5 per water ligand to an average coordination number of 1/6 per water ligand. At

greater distances from the solute, the solvent structure is influenced by the structural changes going along with the oxidation as well. The solvent reorganization beyond the first coordination sphere, however, appears to affect the energy only insignificantly (compare Ref.[28]).

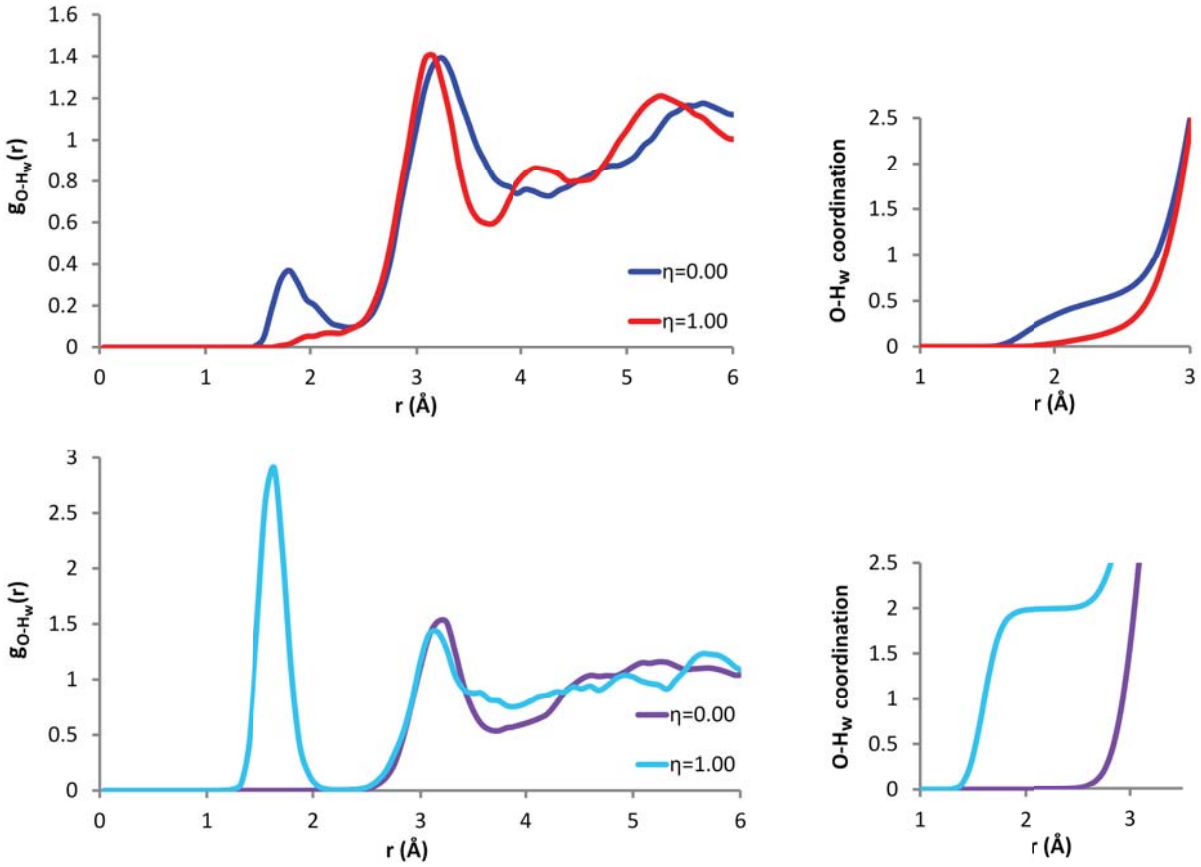

Figure 6: Top left: RDFs between the oxygen atoms of all ligands and the hydrogen atoms of the solvent water molecules for the endstates of the oxidation reaction. Top right: Integral of the displayed RDFs of the oxidation reaction. Bottom left: RDFs between the oxygen atom of the "active" ligand and the hydrogen atoms of the solvent water molecules for the endstates of the deprotonation reaction. Bottom right: Integral of the displayed RDFs of the deprotonation reaction.

The same is not true for the deprotonation reaction, where the removal of a proton can be assumed to strongly influence the H-bonding of the solute with solvent and *vice versa*.[26,28] Indeed, when plotting the RDF between only the oxygen atom of the "active" water ligand and the hydrogen atoms of the solvent water molecules in the protonated ($\eta = 0$) and the fully deprotonated state ($\eta = 1$), we see that the first peak of the RDF in the deprotonated limit is completely absent in the protonated state (lower part of Figure 6). In other words, deprotonation brings the number of H-bonds donated to the "active" ligand (i.e. the O-H_w coordination number) from 0 to 2. The high coordination number in the deprotonated state makes the insertion of a proton, and with that the sampling of the vertical energy gap, quite difficult.

We have shown in Figure 2 that $\langle \Delta_{\mathrm{dp}} E \rangle_{r\eta}$ does not decrease linearly with increasing η. Instead the expectation values of the vertical energy gaps appear to be separated into three groups, the difference between $\eta = 0.75$ and $\eta = 1$ being much larger than between any other consecutive states. As can be seen in Figure 7, $\langle \Delta_{\mathrm{dp}} E \rangle_{r\eta}$ is correlated with the O-H coordination number and changes more strongly with η when the coordination number also changes.[28] The second jump in the number of H-bonds donated to the ligand goes along with a much more strongly pronounced drop in $\langle \Delta_{\mathrm{dp}} E \rangle_{r\eta}$ than the first one, leading to very dissimilar slopes in the protonated and deprotonated limit, which is characteristic for the nonlinear regime. Since the variance of the vertical energy gap is proportional to the slope of $\langle \Delta_{\mathrm{dp}} E \rangle_{r\eta}$ vs. η ($\frac{\partial \langle \Delta_{\mathrm{dp}} E \rangle_{r\eta}}{\partial \eta} = -\frac{\sigma_{r\eta}^2}{k_B T}$),[28] this information can also be extracted from Figure 4. The O-H_w distances in states $\eta = 0.5$ to $\eta = 1$ are approximately 1.6 Å. For such short distances, an additional H-bond significantly reduces the available space and makes proton insertion much more difficult.[26,28] In summary, "[t]he larger the coordination number and the shorter the hydrogen bond, the more nonlinear is the response".[28]

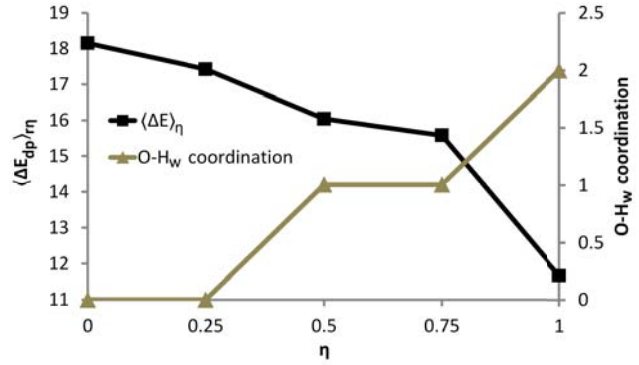

Figure 7: Correlation between changes in the ensemble averages of the vertical energy gaps for the deprotonation reaction with η and changes in the coordination numbers between the oxygen of the "active" ligand and the hydrogen atoms of the solvent water molecules.

Analysis of Errors

The three most significant sources of errors we have not yet considered in our calculations are finite size effects, sampling errors, and the use of a non-hybrid XC functional.

Finite size corrections due to self-interactions scale with the square of the charge of the ions. For Co^{2+} and Co^{3+} these are potentially non-negligible contributions and therefore warrant closer scrutiny. With the procedure described in section Analysis of Errors in the SI, the finite size correction to the dehydrogenation free energy is estimated to be on the order of 0.1 V.

The 95% confidence intervals for the averages of the vertical energy gaps are between $\overline{\Delta E} \pm 30$ meV and $\overline{\Delta E} \pm 80$ meV, with the exception of the DFT-MD simulation sampling the fully deprotonated state (see SI, section Analysis of Errors). As is already obvious from the variance of the vertical energy gap and the convergence behavior of its time average, the standard error of the average is roughly 10 times larger than for the other simulations, which, together with a significantly larger correlation time, leads to a confidence interval of ± 0.5 eV. It

should be mentioned that the time we spent sampling the deprotonated limit (almost 25 ps) is already significantly longer than the ones reported necessary for most other systems.[28,29,86,87]

In contrast to quantum mechanics / molecular mechanics or implicit solvent approaches, the electronic states of the solute can mix with the extended band states of water if they lie energetically close to its band edges, which is not just a property of our method, but a "real" physical effect.[24,85,88] This hybridization is, however, influenced by the delocalization (bandgap) error of the GGA functional,[89] which leads to an underestimation of redox potentials (and indirectly also dehydrogenation energies) by up to approximately 1 eV,[85] but can be reduced significantly by employing hybrid functionals.[24,86] More precisely, the valence band maximum of water is placed at a too high position and (due to hybridization of the solute levels with the band states) the ionization potential of the solute is underestimated.[24,30,85] This effect is most pronounced in species with high, positive redox potentials, and levels close to the valence band maximum of the solvent, but does not strongly depend on hydrogen-bonding, or other structural features.[24,85] Furthermore, misalignment of the water bands leads to a spurious deviation from the linear response regime that could also be mitigated with hybrid functionals.[24,86] For the calculations of deprotonation free energies, on the other hand, GGA functionals perform reasonably well.[30] Finally, we did not find any spin density on the solvent molecules, which would have indicated that the delocalization error had led to the transfer of electron density to the solvent.[28]

It can be concluded that the error made by employing a GGA XC functional is most severe followed by the sampling error in the fully deprotonated state and the finite size error. Unfortunately, all remedies for these issues and possibilities to achieve higher accuracy come at a significantly higher computational cost.

This high computational cost made it impossible for us to employ hybrid functionals in our study, let alone approaches such as many body perturbation methods in the G_0W_0 approximation.[90,91] Fortunately, it may not be necessary to repeat the entire sampling process with a hybrid functional to reduce the error. It has been shown that the H-bond structures obtained with e.g. HSE06 and BLYP are similar,[86] and hence, it might suffice to calculate expectation values of vertical energy gaps from hybrid single point energies of a sufficient number of snapshots along the GGA trajectory.

The large uncertainty of the expectation value of the vertical energy gap in the deprotonated state is a direct consequence of the difficulty in proton insertion due to the solvation structure. The obvious way to tackle this issue and reduce the sampling error is to run an even longer MD trajectory in the deprotonated limit and possibly also calculate ensemble averages of vertical energy gaps in additional states between $\eta = 0.75$ and $\eta = 1$. Furthermore, also the restraining potential might have an influence, and its tuning might warrant further scrutiny.

Since the dominating contribution to our estimation of the finite size error (SI, equation (S46)) is proportional to the inverse volume of the simulation box, increasing the box size along with the number of solvent molecules would quickly reduce its magnitude (but of course increase the computational cost).

Conclusion

We have investigated the calculation of dehydrogenation free energy from DFT-MD for aqueous Co^{II}, which represents the first step in the catalytic cycle of recently investigated Co-

aqua complexes for water oxidation catalysis. Despite the high computational cost of the employed DFT-MD approach for calculating the dehydrogenation free energy of $Co^{II}(H_2O)_6$, the errors in the final result are non-negligible. On the one hand, this is due to issues inherent to the method, and extending the study by calculating single point energies of snapshots along the trajectories with a hybrid functional would substantial improve the accuracy. On the other hand, Co^{II}(aq) is an especially difficult system to simulate due to its high charge, high redox potential and short hydrogen bond lengths in the deprotonated state.

In general, the approach presented in this work provides much more additional information on (dynamic) properties of the investigated systems than standard static calculations using e.g. a solvent continuum model. Moreover, the roadmap to improving its accuracy beyond that provided by the latter approach is in principle clear. Unfortunately, this would demand far more computational resources than can be routinely expended today. For the same reason, an extension of this study to larger WOCs such as biomimetic cubane WOCs is, although desirable, at the moment hardly feasible.

ASSOCIATED CONTENT

Supporting Information. A review of the theory behind the methods used in this work, as well as a detailed description of every step of the calculations can be found in the SI. This material is available free of charge via the Internet at http://pubs.acs.org.

AUTHOR INFORMATION

Corresponding Author

*sandra.luber@chem.uzh.ch

ACKNOWLEDGMENT

We are grateful to Mauro Schilling for discussions and the calculation of the dehydrogenation energy with implicit solvation. We thank the National Center of Competence in Research – Materials Revolution: Computational Design and Discovery of Novel Materials (NCCR-MARVEL) for financial support, and the Swiss National Supercomputing Center (project ID: s502) for computing resources. The work has been supported by the University Research Priority Program "Solar Light to Chemical Energy Conversion" (LightChEC). Funding by Forschungskredit of the University of Zurich, grant no. FK-15-101, is gratefully acknowledged.

REFERENCES

[1] Lewis, N. S. ; Nocera, D. G. *Proc. Natl. Acad. Sci. USA*, **2006**, *103*, 15729-15735.

[2] Berardi, S.; Drouet, S.; Francàs, L.; Gimbert-Surinach, G.; Guttentag, M.; Richmond, C.; Stoll, T; Llobet, A. *Chem. Soc. Rev.*, **2014**, *43*, 7501-7519.

[3] Young, K. J.; Martini, L. A.; Milot, R. L.; Snoeberger, R. C.; Batista, V. S.; Schmuttenmaer, C. A.; Crabtree, R. H.; Brudvig, G. W. *Coord. Chem. Rev*. **2012**, *256*, 2503-2520.

[4] Kanan, M. W.; Nocera, D. G. *Science* **2008**, *321*, 1072-1075.

[5] McAlpin, J. G.; Stich, T. A.; Ohlin, C. A.; Surendranath, Y.; Nocera, D. G.; Casey, W. H.; Britt, R. D. *J. Am. Chem. Soc.* **2011**, *133*, 15444-15452.

[6] McCool, N. S.; Robinson, D. M.; Sheats, J. E.; Dismukes, G. C. *J. Am. Chem. Soc.* **2011**, *133*, 11446-11449.

[7] Berardi, S.; La Ganga, G.; Natali, M.; Bazzan, I.; Puntoriero, F.; Sartorel, A.; Scandola, F.; Campagna, S.; Bonchio, M. J. *J. Am. Chem. Soc.* **2012**, *134*, 11104-11107.

[8] La Ganga, G.; Puntoriero, F.; Campagna, S.; Bazzan, I.; Berardi, S.; Bonchio, M.; Sartorel, A.; Natali, M.; Scandola, F. *Faraday Discuss.* **2012**, *155*, 177-190.

[9] Symes, M. D.; Surendranath, Y.; Luttermann, D. A.; Nocera, D. G. *J. Am. Chem. Soc.* **2011**, *133*, 5174-5177.

[10] Wang, L.-P.; Van Voorhis, T. *J. Phys. Chem. Lett.*, **2011**, *2*, 2200-2204.

[11] Li, X.; Siegbahn, P. E. M. *J. Am. Chem. Soc.* **2013**, *135*, 13804-13813.

[12] Fernando, A.; Aikens, C. M. *J. Phys. Chem. C* **2015**, *119*, 11072-11085.

[13] Ullman, A. M.; Liu, Y.; Huynh, M.; Bediako, D. K.; Wang, H.; Anderson, B. L.; Powers, D. C.; Breen, J. J.; Abruna, H. D.; Nocera, D. G. *J. Am. Chem. Soc.*, **2014**, *136*, 17681-17688.

[14] Genoni, A.; LaGanga, G.; Volpe, A.; Puntoriero, F.; Di Valentin, M.; Bonchio, M.; Natali, M.; Sartorel, A. *Faraday Discuss.* **2015**, *185*, 121−141.

[15] Liu, H.; Schilling, M.; Yulikov, M.; Luber, S.; Patzke, G. R. *ACS Catal.* **2015**, *5*, 4994−4999.

[16] Schilling, M.; Patzke, G. R.; Hutter, J.; Luber, S. *J. Phys. Chem. C*, **2016**, *120*, 7966–7975.

[17] Nørskov, J. K.; Rossmeisl, J.; Logadottir, A.; Lindqvist, L.; Kitchin, J. R.; Bligaard, T.; Jonsson, H. *J. Phys. Chem. B* **2004**, *108*, 17886-17892.

[18] Rossmeisl, J.; Logadottir, A.; Nørskov, J. K. *Chem. Phys.* **2014**, *319*, 178-184.

[19] Rossmeisl, J.; Nørskov, J. K *J. Phys. Chem. B* **2006**, *110*, 21833-21839.

[20] Rossmeisl, J.; Qu, Z.W.; Zhu, Q.; Kroes, G.-J.; Nørskov, J. K. *J. Electroanal. Chem. B* **2007**, *607*, 83-89.

[21] Hohenberg, P.; Kohn, W. *Phys. Rev.* **1964**, *136*, B864–B871.

[22] Kohn, W.; Sham, L. J. *Phys. Rev.* **1965**, *140*, A1133–A1138.

[23] Blumberger, J.; Tavernelli, I.; Klein, M. L.; Sprik, M. *J. Chem. Phys.* **2006**, *124*, 064507.

[24] Adriaanse, C.; Cheng, J.; Chau, V.; Sulpizi, M.; VandeVondele, J.; Sprik, M. *J. Phys. Chem. Lett*. **2012**, *3*, 3411−3415.

[25] Blumberger, J.; Sprik, M. *Theor. Chem. Acc.* **2006**, *115*, 113-126.

[26] Sulpizi, M.; Sprik, M. *Phys. Chem. Chem. Phys.* **2008**, *10*, 5238-5249.

[27] Tateyama, Y.; Blumberger, J.; Sprik, M.; Tavernelli, I. *J. Chem. Phys.* **2005,** *122,* 234505.

[28] Cheng, J.; Sulpizi, M.; Sprik, M. *J. Chem. Phys.* **2009,** *131,* 154504.

[29] Costanzo, F.; Sulpizi, M.; Della Valle, R. G.; Sprik, M. *J. Chem. Phys.* **2011,** *134,* 244508.

[30] Cheng, J.; Liu, X.; VandeVondele, J.; Sulpizi, M.;Sprik, M. *Acc. Chem. Res.* **2014,** *47*, 3522–3529.

[31] Mangold, M.; Rolland, L.; Costanzo, F.; Sprik, M.; Sulpizi, M.; Blumberger, *J. Chem. Theory Comput.* **2011**, *7*, 1951-1961.

[32] Warshel, A. *J. Phys. Chem.* **1982**, *86*, 2218-2224.

[33] King, G.; Warshel, A. *J. Chem. Phys.* **1990**, *93*, 8682-8692.

[34] Evangelisti, F.; Güttinger, R.; More, R.; Luber, S.; Patzke, G. R. *J. Am. Chem. Soc.* **2013**, *135*, 11076–11084.

[35] Evangelisti, F.; More, R.; Hodel, F.; Luber, S.; Patzke, G. R. *J. Am. Chem. Soc.* **2015**, *137*, 18734–18737.

[36] Hodel, F. H.; Luber, S. *ACS Catal*. **2016**, *6*, 1505-1517.

[37] Hodel, F. H.; Luber, S. *ACS Catal*. **2016,** *6*, 6750-6761.

[38] Hodel, F. H.; Luber, S. *submitted*.

[39] Tomasi, J.; Mennucci, B.; Cammi, R. *Chem. Rev.* **2005**, *105*, 2999−3094.

[40] Marenich, A. V.; Ho, J.; Coote, M. L.; Cramer, C. J.; Truhlar, D. G. *Phys. Chem. Chem. Phys.* **2014**, *16*, 15068−15106.

[41] Marcus, R. A. *J. Chem. Phys.* **1956,** *24, 966*–978.

[42] Marcus, R. A. *J. Chem. Phys.* **1956**, *24*, 979–988.

[43] Marcus, R. A. *Discuss. Faraday Soc*. **1960***, 29*, 21-31.

[44] Marcus, R. A. *J. Chem. Phys*. **1965**, *43*, 679-701.

[45] Marcus, R. A. *Rev. Mod. Phys.* **1993**, *65,* 599–610.

[46] Frenkel, D.; Smit, B. *Understanding Molecular Simulations: From Algorithms to Applications*, 2nd ed.; Academic Press, San Diego, 1996.

[47] Chipot, C.; Pohorille, A. *Free Energy Calculations: Theory and Applications in Chemistry and Biology*, Series in Chemical Physics Vol. 86 Springer, New York, 2006.

[48] VandeVondele, J.; Krack, M.; Mohamed, F.; Parrinello, M.; Chassaing, T.; Hutter, J. *J. Comp. Phys. Comm.* **2005** *167*, 103-128.

[49] CP2K Developers Group, URL: http://www.cp2k.org.

[50] Bussi, G.; Donadio, D.; Parrinello, M. *J. Chem. Phys.* **2007**, *126*, 014101.

[51] Brooks, B. R.; Brooks, C. L.; Mackerell, A. D.; Nilsson, L.; Petrella, R. J.; Roux, B.; Won, Y.; Archontis, G.; Bartels, C.; Boresch, S.; Caflisch, A.; Caves, L.; Cui, Q.; Dinner, A. R.; Feig, M.; Fischer, S.; Gao, J.; Hodoscek, M.; Im, W.; Kuczera, K.; Lazaridis, T.; Ma, J.; Ovchinnikov, V.; Paci, E.; Pastor, R. W.; Post, C. B.; Pu, J. Z.; Schaefer, M.; Tidor, B.; Venable, R. M.; Woodcock, H. L.; Wu, X.; Yang, W.; York, D. M.; Karplus, M. *J. Comput. Chem.* **2009**, 30, 1545-1614.

[52] Jorgensen, W. L.; Chandrasekhar, J.; Madura, J. D.; Impey, R. W.; Klein, M. L. *J. Chem. Phys.* **1983**, *79*, 926-935.

[53] Blumberger, J.; Bernasconi, L.; Tavernelli, I.; Vuilleumier, R.; Sprik, M. *J. Am. Chem. Soc.*, **2004**, *126*, 3928–3938.

[54] Bill, E.; Bothe, E.; Chaudhuri, P.; Chlopek, K.; Herebian, D.; Kokatam, S.; Ray, K.; Weyhermüller, T.; Neese, F.; Wieghardt, K. *Cem. Eur. J.* **2005**, *11*, 204-224.

[55] Ames, W.; Pantazis, D. A.; Krewald, V.; Cox, N.; Messinger, J.; Lubitz, W.; Neese, F. *J. Am. Chem. Soc.* **2011**, *133*, 19743-19757.

[56] Orio, M.; Pantazis, D. A.; Neese, F. *Photosynth. Res.* **2009**, *102*, 443-453.

[57] Neese, F. J. *Biol. Inorg. Chem.* **2006**, *11*, 702-707.

[58] Neese, F. *Coord. Chem. Rev.* **2009**, *253*, 526-563.

[59] Neese, F.; Ames, W.; Christian, G.; Kampa, M.; Liakos, D. G.; Pantazis, D. A.; Roemelt, M.; Surawatanawong, P.; Ye, S. F. *Adv. Inorg.Chem.* **2010**, *62*, 301-349.

[60] Bühl, M. *Inorg. Chem.*, **2005**, *44*, 6277–6283.

[61] VandeVondele, J.; Hutter, J. *J. Chem. Phys.* **2007** *127*, 114105.

[62] Goedecker, S.; Teter, M.; Hutter, J. *Phys. Rev. B* **1996** *54*, 1703-1710.

[63] Hartwigsen, C.; Goedecker, S.; Hutter, J. *Phys. Rev. B* **1998**, *58*, 3641-3662.

[64] Grimme, S.; Antony, J.; Ehrlich, S.; Krieg, H. *J. Chem. Phys.* **2010**, *132*, 154104.

[65] Siegbahn, P. E. M.; Blomberg, M. R. A.; Chen, S.-C. *J. Chem. Theory Comput.* **2010**, *6*, 2040-2044.

[66] Wang, J.; Roman-Perez, G. ; Soler, J. M. ; Artacho, E. ; Fernandez-Serra, M.-V. *J. Chem. Phys.* **2011**, *134*, 024516.

[67] Schmidt, J.; VandeVondele, J.; Kuo, I.-F. W.; Sebastiani, D.; Siepmann, J. I.; Hutter, J.; Mundy, C. J. *J. Phys. Chem. B* **2009**, *113*, 11959-11964.

[68] VandeVondele, J.; Mohamed, F.; Krack, M.; Hutter, J.; Sprik, M.; Parrinello, M. *J. Chem. Phys.* **2005**, *122*, 014515.

[69] Jonchiere, R.; Seitsonen, A. P.; Ferlat, G.; Saitta, A. M.; Vuilleumier, R. *J. Chem. Phys.* **2011**, *135*, 154503.

[70] Liu, X.; Lu, X.; Sprik, M.; Cheng, J.; Meijer, E. J.; Wang, R. *Geochim. Cosmochim. Acta* **2013**, *117*, 180-190.

[71] Sulpizi, M.; Sprik, M. *J. Phys. Condens. Matter* **2010**, *22*, No. 284116.

[72] Uudsemaa, M.; Tamm,T. *J. Phys. Chem. A* **2003**, *107*, 9997−10003.

[73] Gütlich, P.; Goodwin, H. A. *Spin Crossover in Transition Metal Compounds II*, 1st ed.; Springer, 2004.

[74] Luther, G. W. *Inorganic Chemistry for Geochemistry and Environmental Sciences*, 1st ed.; Wiley: Chichester, 2016.

[75] Ebbing, D. D., *General Chemistry*, 3rd ed., Houghton Mifflin: Boston, 1990.

[76] Sisley, M. J.; Jordan, R. B. *Inorg. Chem.* **2006**, *45*, 10758-10763.

[77] Ho, J.; Coote, M. L.; Cramer, C. J.; Truhlar, D. G. *Theoretical calculation of reduction potentials.* In *Organic Electrochemistry*, 5th edition; Hammerich, O., Speiser, M., Eds.; CRC Press, Boa Raton, FL, 2016; pp. 229-259.

[78] Ho, J. *Aust. J. Chem.* **2014**, *67*, 1441-1460.

[79] Ayala, R.; Sprik, M. *J. Phys. Chem. B*, **2008**, *112*, 257-269.

[80] Zhou, H.-X.; Szabo, A. *J. Chem. Phys.* **1995**, *103*, 3481-3494.

[81] Blumberger, J. *J. Am. Chem. Soc.*, **2008**, *130*, 16065–16068.

[82] Jahn, H. A.; Teller, E. *Proc. R. Soc. Lond.* **1937**, *A161*, 220-225.

[83] Jahn, H. A. *Proc. R. Soc. Lond.* **1938**, *A164*, 117-131.

[84] Huheey, J. E.; Keiter, E. A.; Keiter, R. L. *Inorganic Chemistry: Principles of Structure and Reactivity*, 4th ed.; HarperCollins: New York, 1993.

[85] Kallies, B.; Meier, B. *Inorg. Chem.* **2001**, *40*, 3101-3112.

[86] Liu, X.; Cheng, J.; Sprik, M. *J. Phys. Chem. B* **2015**, *119*, 1152-1163.

[87] Liu, X.; Cheng, J.; Lu, X.; He, M.; Wang, R. *Phys. Chem. Chem. Phys.* **2016**, **DOI:** 10.1039/C6CP01375A

[88] Winter, B.; Faubel, M.; Hertel, I. V.; Pettenkofer, C.; Bradforth, S. E.; Jagoda-Cwiklik, B.; Cwiklik, L.; Jungwirth, P. *J. Am. Chem. Soc*. **2006**, *128*, 3864-3865.

[89] Mori-Sánchez, P.; Cohen, A. J.; Yang, W. *Phys. Rev. Lett.* **2008**, *100*, 146401-146404.

[90] Pham, T. A.; Zhang, C.; Schwegler, E.; Galli, G. *Phys. Rev. B* **2014**, *89*, 060202.

[91] Opalka, D.; Pham, T.; Sprik, M.; Galli, G. *J. Chem. Phys.* **2014**, *141*, 034501.

For Table of Contents Use Only

Dehydrogenation Free Energy of Co^{2+}(aq) from Molecular Dynamics

*Florian H. Hodel and Sandra Luber**